Modulation Concepts for the Control of a Two-Phase Bearingless Slice Motor Utilizing Three-Phase Power Modules

Martin T. Bartholet, *Member, IEEE*, Thomas Nussbaumer, *Member, IEEE*, Daniel Krähenbühl, *Student Member, IEEE*, Franz Zürcher, *Student Member, IEEE*, and Johann W. Kolar, *Fellow, IEEE*

***Abstract*—Future application areas for bearingless pump systems will demand for highly compact and cost effective designs. This trend mainly has a major impact on the power electronics part of these systems. Up to now, full-bridge converters have been used in order to independently control the phases of the active magnetic bearing and the drive system. With the use of an interleaved half-bridge topology, the number of required power semiconductors is reduced by 25%. In this paper, novel modulation techniques are presented and comparatively evaluated in order to achieve a similar dynamic performance of the pump system as with the conventional full-bridge topology. The effects of a phase shift and of higher harmonics in the duty cycles are analyzed in detail. The proposed concepts are then implemented on a DSP board, and their feasibility is shown on a highly compact 1.5-kW prototype of the converter which is realized with two integrated three-phase power modules. Furthermore, it is shown that the higher harmonics injection does not have an impact on the average speed of the impeller and thus on the constant output flow of the pump.**

***Index Terms*—Bearingless motor, fluid handling, magnetic levitation, modulation methods, power electronics.**

I. Introduction

NEW APPLICATION areas for bearingless pump systems such as electroplating, the food industry, as well as in the area of the biotechnology [1] require the development of very compact and cost-efficient converter designs for the bearingless slice motor (BSM) system [2]. The various benefits of the bearingless pump for the handling of very pure and aggressive fluids in the semiconductor industry and for medical applications are described in [3]. However, in order to attract new markets for the BSM technology, the whole system must become economically more attractive. Research, so far, has only been carried out on the motor itself, and very little research effort has been focused on the investigation of novel converter topologies to control the drive and bearing system.

In a first approach, a novel topology for the control of the two-phase BSM system has been presented in [4] which decreases the number of required semiconductors by 25%. By connecting two drive/bearing windings to common bridge legs and utilizing three-phase power modules [cf., Fig. 1(b)], which are available off-the-shelf, a higher efficiency and a more compact design of the power electronics part can be achieved. Based on this, different modulation schemes for the control of the pump with the interleaved half-bridge topology are investigated and assessed in this paper.

The BSM utilized in this paper has a symmetrical winding configuration with two bearing phases L_{B1} and L_{B2} and two drive phases L_{D1} and L_{D2}, as shown in Fig. 2. The stabilization of the rotor is realized with contactless magnetic bearings that are placed around eight claws which are carrying the flux of the bearing and drive system. The control of the current in each drive and bearing winding, and thus the flux, is up to now performed by one separate full-bridge converter for each phase. This results in a total number of 16 power transistor/diode combinations for the converter [cf., Fig. 1(a)]. The orthogonal placement of the coils in the motor yields a $\pi/2$ phase shift of the currents in the drive windings under operation.

This paper presents and comparatively evaluates different modulation schemes for the interleaved half-bridge topology for the control of the BSM. First, the derivation of the interleaved half-bridge topology from the state-of-the-art full-bridge topology is briefly presented in Section II. Starting with a constant common bridge leg modulation (CCM), a more advanced modulation scheme with sinusoidally shaped common bridge leg duty cycles, and an optimum phase shift between all bridge leg duty cycles is then derived in Section III. In addition, the superposition of higher harmonics to the sinusoidally modulated duty cycles and their impact on the drive currents is presented. Section IV deals with the aspect of speed unbalances due to the before mentioned higher harmonics in the drive current and proves the theoretical considerations by measurements on a pump system. The maximum achievable drive power is then discussed in Section V for the proposed modulation schemes.

Paper 2008-IDC-069.R1, presented at the 2007 Power Conversion Conference, Nagoya, Japan, April 2–5, and approved for publication in the IEEE TRANSACTIONS ON INDUSTRY APPLICATIONS by the Industrial Drives Committee of the IEEE Industry Applications Society. Manuscript submitted for review January 16, 2009 and released for publication September 3, 2009. First published February 5, 2010; current version published March 19, 2010.

M. T. Bartholet is with Celeroton AG, 8092 Zurich, Switzerland (e-mail: martin.bartholet@celeroton.com).

T. Nussbaumer is with Levitronix GmbH, 8005 Zurich, Switzerland (e-mail: nussbaumer@levitronix.com).

D. Krähenbühl and J. W. Kolar are with the Power Electronic Systems Laboratory, Swiss Federal Institute of Technology (ETH) Zurich, ETH Zentrum/ETL H23, 8092 Zurich, Switzerland (e-mail: kraehenbuehl@lem.ee.ethz.ch; kolar@lem.ee.ethz.ch).

F. Zürcher is with the Power Electronic Systems Laboratory, Swiss Federal Institute of Technology Zurich, 8005 Zurich, Switzerland (e-mail: zurcher@lem.ee.ethz.ch).

Digital Object Identifier 10.1109/TIA.2010.2041089

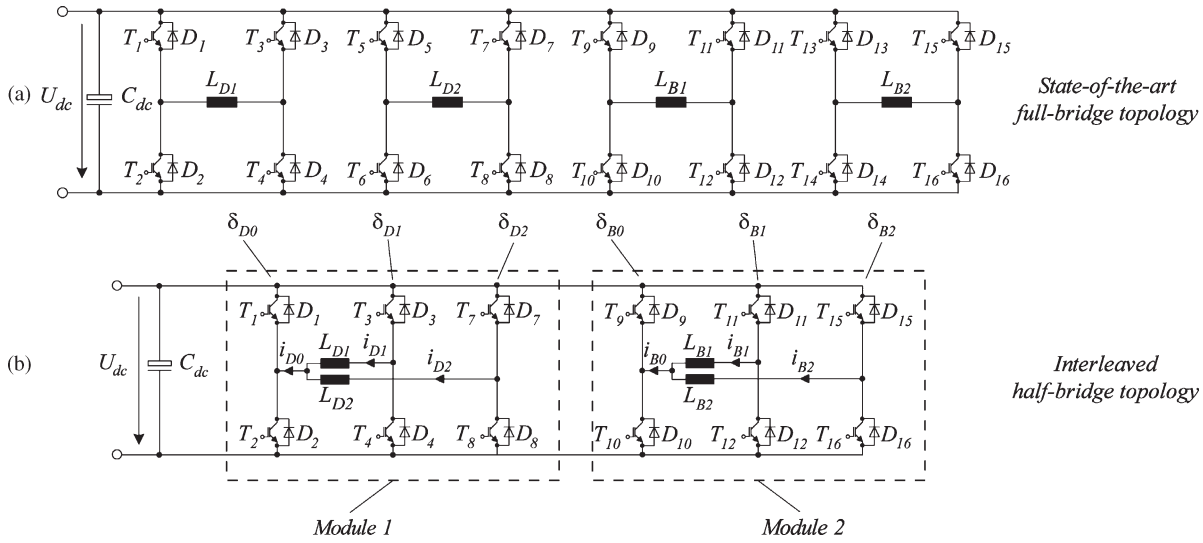

Fig. 1. Possible power electronic interfaces. (a) State-of-the-art full-bridge topology for BSM for each drive (L_{Di}) and bearing (L_{Bi}) winding. (b) Interleaved half-bridge topology with two common bridge legs for the two drive (L_{D1}, L_{D2}) and bearing (L_{B1}, L_{B2}) systems.

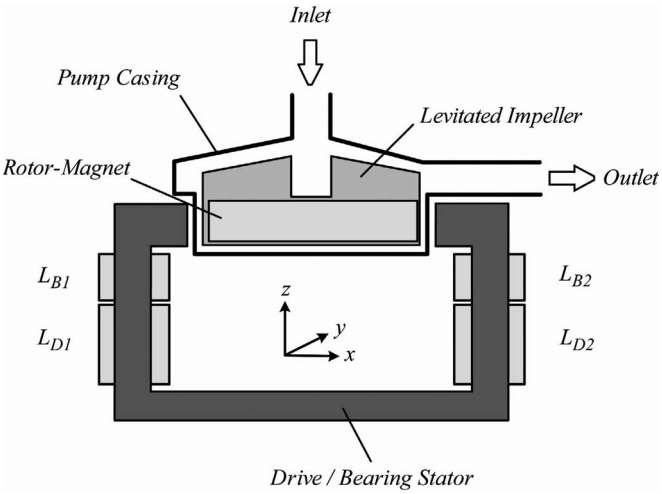

Fig. 2. Schematic of the basic principle of the bearingless centrifugal pump.

Finally, in Section VI, the modulation schemes are verified by measurements on a 1.5-kW prototype of the converter with a pump system.

II. Interleaved Half-Bridge Topology

In Fig. 1(a), the state-of-the-art converter topology for the control of the drive and bearing currents of the two-phase BSM is shown. As described in detail in [3], the number of power semiconductors can be reduced if the power transistor/diode combinations T_5/D_5 and T_6/D_6 of the left bridge leg of the drive winding L_{D2} are removed. The two drive windings are now connected together with the junction of the bridge leg T_1/D_1 and T_2/D_2 [cf., Fig. 1(b)]. This leg is used as the common bridge leg for the drive system. With this setup, the control of the drive system is realized by three interleaved half-bridges.

The same is done, in a similar way, with the two bearing windings. Here, the combinations T_{13}/D_{13} and T_{14}/D_{14} are removed and the bearing windings are connected to the second common bridge leg consisting of the insulated gate bipolar transistors (IGBTs) and diodes T_9/D_9 and T_{10}/D_{10}. This circuit allows a realization of the converter with only six power half-bridges, resulting in a total of 12 switches, by offering a similar control flexibility as the full-bridge converter as will be described in this paper later on. With the use of this interleaved half-bridge topology, the total amount of switches needed to control the BSM is reduced by one fourth compared to the state-of-the-art full-bridge topology.

The idea of component minimization due to the connection of more than one motor winding to a common bridge leg has also been investigated in the area of the control of induction machines [5]–[10]. In [5], a five-leg inverter is used to supply two three-phase induction machines. One leg of the five-leg inverter is simultaneously connected to both machines while the remaining inverter legs are connected to the two machines only. However, as it is the case for the before mentioned control of induction machines [11], [12], new modulation schemes must be developed in order to achieve a similar performance and dynamical behavior of the pump system as it is obtained with the standard full-bridge topology. Therefore, in the following section, different modulation concepts are presented and evaluated comparatively.

III. Modulation Methods

In this section, different modulation methods for the interleaved half-bridge topology [cf., Fig. 1(b)] for the control of a BSM are analyzed. First, a basic modulation with lowest control effort is presented. Then, alternative modulation methods are characterized in order to provide higher modulation depth and therefore better motor performance. In literature, the addition of higher harmonics to the output waveforms of an inverter is intensively considered under the aspect of lowering the losses and thus minimizing the overheating of the motor as well as reducing the vibrations in the motor [13]–[15]. However, in the hereafter presented work, the main focus lies on the maximum achievable drive power obtainable by the addition

of higher harmonics to the fundamental waveform and the resulting operation behavior of the BSM.

The average voltages $\overline{u}_{D1}(t)$ and $\overline{u}_{D2}(t)$ of the drive coils are defined as

$$\begin{aligned}\overline{u}_{D1}(t) &= U_{dc} \cdot (\delta_{D1} - \delta_{D0}) = m \cdot U_{dc} \cdot \cos \omega t \\ \overline{u}_{D2}(t) &= U_{dc} \cdot (\delta_{D2} - \delta_{D0}) = m \cdot U_{dc} \cdot \sin \omega t \end{aligned} \quad (1)$$

where the modulation depth m is defined as

$$m = \frac{\overline{u}_{\max}}{U_{dc}} = 0, \ldots, m_{\max} \quad (2)$$

with $m_{\max} = 0.95$. This corresponds to the maximum value allowed to ensure a safe operation of the system.

Moreover, U_{dc} stands for the dc-link voltage and δ_{D0}, δ_{D1}, and δ_{D2} are the duty cycles applied to the upper switches in each bridge leg of the drive module [cf., Fig. 1(b)]. The duty cycles of the lower switches are then given by $(1 - \delta_{Di})$ with $i = 0, 1, 2$. In the following, only the expression δ_{Di} is used to describe the duty cycles of the bridge legs. Furthermore, $\overline{u}_{\max}$ is the maximum value of the average voltage (local average value over one pulse period) at the junction point of a bridge leg. Analogously, the duty cycles δ_{B0}, δ_{B1}, and δ_{B2} are applied to the upper switches of the bearing module in Fig. 1(b). The interleaved half-bridge converter is operated with unipolar modulation as it is described in [16].

Due to the fact that the major part of the power consumption is taken by the drive system, the requirements regarding the modulation range are higher for the drive part. Hence, different modulation concepts are discussed for the drive system in the following. However, the considerations are also valid for the modulation of the bearing currents.

A. CCM

In this basic modulation scheme, the duty cycle δ_{D0} of the common bridge leg is kept constant at $\delta_{D0} = 0.5$. This leads to an average potential of $U_{dc}/2$ at the connection point of the two windings. In addition, the duty cycles δ_{D1} and δ_{D2} are sinusoidally modulated with

$$\begin{aligned}\delta_{D1} &= \frac{1}{2} + \frac{m}{2} \cos(\omega\, t) \\ \delta_{D2} &= \frac{1}{2} + \frac{m}{2} \sin(\omega\, t). \end{aligned} \quad (3)$$

This is shown in Fig. 3. Furthermore, the resulting voltages $\overline{u}_{D1}(t)$ and $\overline{u}_{D2}(t)$

$$\begin{aligned}\overline{u}_{D1}(t) &= \frac{m}{2} \cdot U_{dc} \cdot \cos \omega t \\ \overline{u}_{D2}(t) &= \frac{m}{2} \cdot U_{dc} \cdot \sin \omega t \end{aligned} \quad (4)$$

and currents $i_{D0}(t)$, $i_{D1}(t)$, and $i_{D2}(t)$ of the two drive windings are shown in Fig. 3 as well. For the derivation of these curves, the values of the drive inductances $L_{D1} = L_{D2} = 35$ mH of the prototype system of the BSM have been used (the very small drive resistance can be neglected). It can be seen

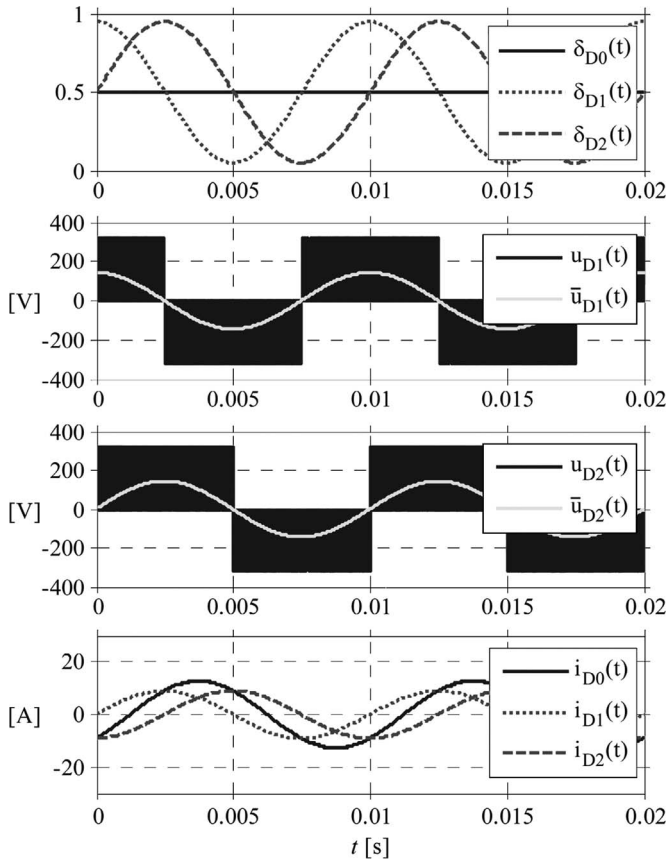

Fig. 3. Simulation results for CCM. Duty cycles δ_{D0}, δ_{D1}, and δ_{D2}, switched voltage u_{D1} and average voltage $\overline{u}_{D1}$ across coil L_{D1}, switched voltage u_{D2} and average voltage $\overline{u}_{D2}$ across coil L_{D2}, and currents i_{D0}, i_{D1}, and i_{D2} of the drive system.

that the maximum average voltage across a drive coil obtainable with the described modulation scheme is given by

$$\overline{u}_{D\max} = m_{\max} \cdot \frac{U_{dc}}{2}. \quad (5)$$

Compared to the conventional modulation of the full-bridge topology [cf., Fig. 1(a)], this voltage is therefore reduced by a factor of two. This value is sufficient when only looking at the bearing system, and its demands regarding a stable operation of the pump. In this case, the maximum rms bearing current that arises when the pump is operated with the maximum phase voltage, which equals half the dc-link voltage, is 2.7 A. However, for the drive system, where high voltages across the coils are needed in order to deliver high pump power, this performance decrease is unacceptable. Even more, the theoretical maximum rms drive phase current would increase to 10.4 Arms in this case. Therefore, in the following, different modulation schemes are developed which provide higher modulation ratios as the one obtained with CCM, and, with this, also the maximum drive current will be decreased.

B. SCM

An increased modulation ratio is achievable for the drive system if the duty cycle δ_{D0} of the power switch T_1 [cf., Fig. 1(b)] in the common bridge leg is varied sinusoidally.

For the calculation of the required duty cycle, we assume that the gate signals of all switches are phase shifted by the angle φ_0

$$\delta_{D0} = \frac{1}{2} + \frac{m}{2}\sin(\omega\, t + \varphi_0) \tag{6}$$

and that δ_{D1} and δ_{D2} are symmetrically distributed with respect to δ_{D0} by the angle $\Delta\varphi$

$$\begin{aligned}\delta_{D1} &= \frac{1}{2} + \frac{m}{2}\sin(\omega\, t + \varphi_0 - \Delta\varphi)\\ \delta_{D2} &= \frac{1}{2} + \frac{m}{2}\sin(\omega\, t + \varphi_0 + \Delta\varphi).\end{aligned} \tag{7}$$

A symmetrical distribution of δ_{D1} and δ_{D2} versus ωt is chosen due to the fact that the same modulation depth for both drive windings is desired.

In the following, the calculation of the optimal values of φ_0 and $\Delta\varphi$ for highest modulation depth is presented. Combining (1), (6), and (7) results in the following expression for $\overline{u}_{D1}(t)$:

$$\begin{aligned}\overline{u}_{D1}(t) &= m \cdot U_{dc}\cos\left(\omega\, t + \varphi_0 - \frac{\Delta\varphi}{2}\right)\sin\left(-\frac{\Delta\varphi}{2}\right)\\ &= m \cdot U_{dc}\cos\omega\, t.\end{aligned} \tag{8}$$

Analogously, $\overline{u}_{D2}(t)$ can be calculated as

$$\begin{aligned}\overline{u}_{D2}(t) &= m \cdot U_{dc}\cos\left(\omega\, t + \varphi_0 + \frac{\Delta\varphi}{2}\right)\sin\left(\frac{\Delta\varphi}{2}\right)\\ &= m \cdot U_{dc}\sin\omega\, t.\end{aligned} \tag{9}$$

Solving (7) and (8) for φ_0 and $\Delta\varphi$ leads to

$$\begin{aligned}\varphi_0 &= -\frac{3\pi}{4}\\ \Delta\varphi &= \frac{\pi}{2}\end{aligned} \tag{10}$$

and therefore to the following expressions for δ_{D0}, δ_{D1}, and δ_{D2}:

$$\begin{aligned}\delta_{D0} &= \frac{1}{2} + \frac{m}{2}\sin\left(\omega\, t - \frac{3\pi}{4}\right) = \frac{1}{2} - \frac{m}{2}\cos\left(\omega t - \frac{\pi}{4}\right)\\ \delta_{D1} &= \frac{1}{2} + \frac{m}{2}\sin\left(\omega\, t - \frac{5\pi}{4}\right) = \frac{1}{2} - \frac{m}{2}\sin\left(\omega t - \frac{\pi}{4}\right)\\ \delta_{D2} &= \frac{1}{2} + \frac{m}{2}\sin\left(\omega\, t - \frac{\pi}{4}\right) = \frac{1}{2} + \frac{m}{2}\sin\left(\omega t - \frac{\pi}{4}\right)\end{aligned} \tag{11}$$

and for $\overline{u}_{D1}(t)$ and $\overline{u}_{D2}(t)$

$$\begin{aligned}\overline{u}_{D1}(t) &= \frac{m}{\sqrt{2}} \cdot U_{dc} \cdot \cos\omega t\\ \overline{u}_{D2}(t) &= \frac{m}{\sqrt{2}} \cdot U_{dc} \cdot \sin\omega t.\end{aligned} \tag{12}$$

With this, the new duty cycles δ_{D1} and δ_{D2} are phase shifted by π while the angle between the winding currents $i_{D1}(t)$ and $i_{D2}(t)$ remains $\pi/2$ (cf., Fig. 4). As shown in (12), the voltages across the drive coils achievable with the sinusoidal common bridge leg modulation (SCM) scheme are increased by a factor of $\sqrt{2}(= +41\%)$ as compared to the CCM method.

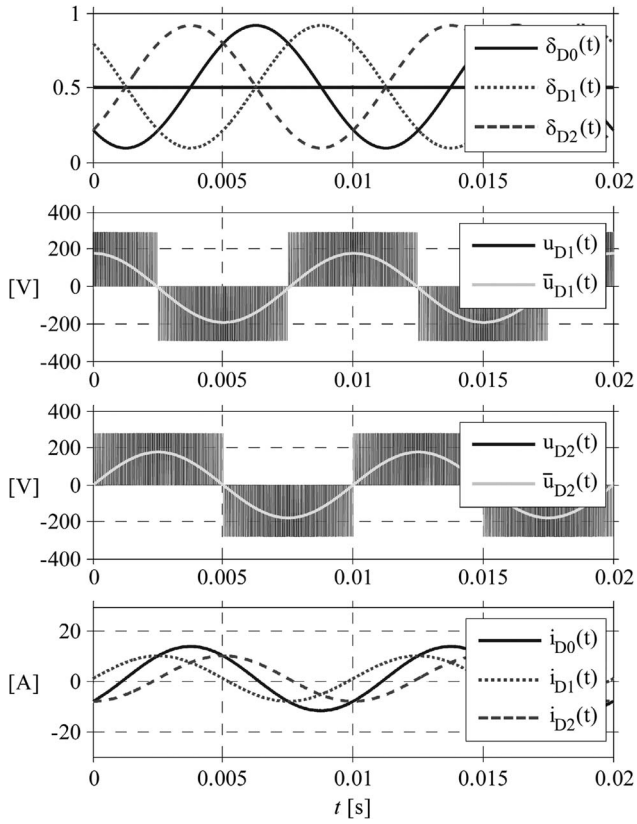

Fig. 4. Simulation results for SCM. Duty cycles δ_{D0}, δ_{D1}, and δ_{D2}, switched voltage u_{D1} and average voltage $\overline{u}_{D1}$ across coil L_{D1}, switched voltage u_{D2} and average voltage $\overline{u}_{D2}$ across coil L_{D2}, and currents i_{D0}, i_{D1}, and i_{D2} of the drive system.

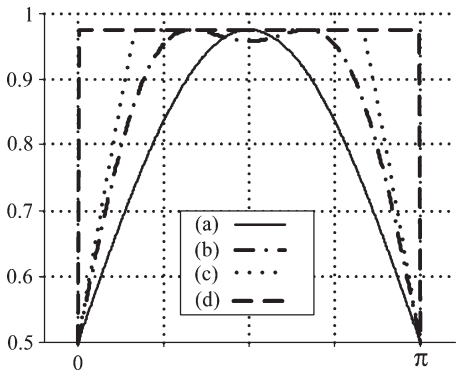

Fig. 5. Duty cycle waveform for (a) purely sinusoidal, (b) third harmonic, (c) constant 120°, and (d) full square wave modulation.

C. Harmonic Injection

Following the concept of the SCM (Section III-B), additional higher harmonics can be superposed to the common bridge leg duty cycle in order to further increase the modulation depth. The method of distorting the phase voltages by adding third harmonics first been presented in [18] for three-phase induction machines. As will be shown in the following, this method also works fine for the interleaved-half-bridge topology at hand. Furthermore, it will be shown in the subsequent sections that additional higher harmonics may further increase the available phase voltage and thus, the performance of the converter. In a first approach, a third harmonic is superposed to

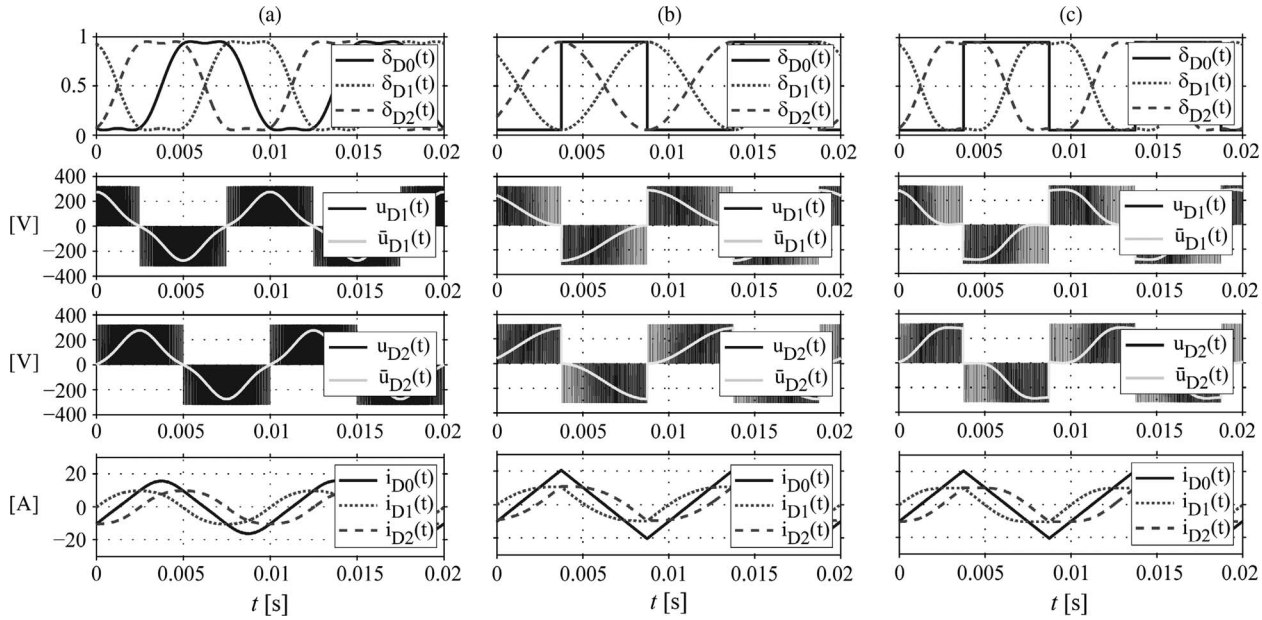

Fig. 6. Simulation results for (a) THM, (b) QCM, and (c) TQM with duty cycles δ_{D0}, δ_{D1}, and δ_{D2}, switched voltage u_{D1} and average voltage $\overline{u}_{D1}$ across coil L_{D1}, switched voltage u_{D2} and average voltage $\overline{u}_{D2}$ across coil L_{D2}, and currents i_{D0}, i_{D1}, and i_{D2} of the drive system.

a purely sinusoidal duty cycle to provide a higher utilization of the dc bus voltage. The amount of the third harmonic and the fundamental component is chosen so that the latter is maximized while ensuring that the peak-to-peak amplitude does not exceed the maximum allowed modulation depth. The corresponding average duty cycle is shown in Fig. 5(b). With this, the voltage–time product is increased compared to purely sinusoidal modulation. Adding additional higher harmonics to the sinusoidal fundamental subsequently leads to a full square wave modulation, as shown in the waveform in Fig. 5(d).

Alternatively to the modulation schemes with harmonic injection, the duty cycle can also be simply limited to the maximum applicable modulation depth over a certain amount of time (e.g., 120°) and keep it linearly increasing at the beginning and linearly decreasing at the end of a half-period [Fig. 5(c)]. This method is commonly denominated as flat-top modulation and can be regarded as a compromise between third harmonic injection [Fig. 5(b)] and full square wave modulation [Fig. 5(d)] and will not be investigated in the following to keep the focus on the essentials.

1) THM: Applying the previously discussed concept of the superposition of a third harmonic to each of the duty cycles, while keeping the same phase shift as it is defined for SCM, leads to another modulation concept denominated as third harmonic modulation (THM). The resulting duty cycles δ_{D0}, δ_{D1}, and δ_{D2} of the three half-bridges are

$$\begin{aligned}
\delta_{D0} &= \frac{1}{2} - \frac{m}{\sqrt{3}}\cos\left(\omega t - \frac{\pi}{4}\right) + \frac{m}{6\sqrt{3}}\cos\left(3\omega t - \frac{3\pi}{4}\right) \\
\delta_{D1} &= \frac{1}{2} - \frac{m}{\sqrt{3}}\sin\left(\omega t - \frac{\pi}{4}\right) - \frac{m}{6\sqrt{3}}\sin\left(3\omega t - \frac{3\pi}{4}\right) \\
\delta_{D2} &= \frac{1}{2} + \frac{m}{\sqrt{3}}\sin\left(\omega t - \frac{\pi}{4}\right) + \frac{m}{6\sqrt{3}}\sin\left(3\omega t - \frac{3\pi}{4}\right).
\end{aligned} \tag{13}$$

The duty cycle, voltage and current waveforms for the THM method are shown in Fig. 6(a). Analogously to (11), the fundamental sine waves are phase shifted by $\pi/4$, whereas the superposed third harmonics show a phase shift of $3\pi/4$. Furthermore, in order to achieve maximum modulation depth, the fundamental waveform has to be multiplied by $2/\sqrt{3}$ while the third harmonics are multiplied by $1/(6\sqrt{3})$. With this, the maximum appearing duty cycle is still maintained to be one, while the first harmonic of the drive voltage is increased by a factor of $2/\sqrt{3}(=+15\%)$ compared to purely sinusoidal modulation (SCM). Compared to CCM, this means an improvement of 63%. A drawback of this control technique clearly is that the currents in the windings are no longer not sinusoidal. This issue will be further investigated in Section IV.

2) QCM: Unlike the previously presented modulation schemes for the square common bridge leg modulation (QCM), the duty cycle of the common bridge leg δ_{D0} is of rectangular shape [cf., Fig. 6(b)] with the same phase shift φ_0 as it has been used for THM and SCM. This modulation of the common bridge leg represents the maximum quantity of superposed higher harmonics which leads to a full square wave. The average duty cycles δ_{D1} and δ_{D2} are sinusoidally modulated and show a phase shift of $\pi/2$. The maximum amplitude of the fundamental harmonic of the applied drive voltage is increased by 62% compared to the one achieved with CCM.

3) Third Harmonic and Square Common Bridge Leg Modulation (TQM): A further increase in the maximum available drive voltage can be achieved when combining the idea of the THM and the QCM. This leads to a square wave modulation of the duty cycle in the common bridge δ_{D0} while superposing third harmonics to the sinusoidal fundamental of the duty cycles δ_{D1} and δ_{D2} as it is shown in Fig. 6(c). With this modulation scheme, the fundamental drive voltage is increased by 72% compared to CCM. As shown in Fig. 6, the resulting current waveform [cf., Fig. 6(c)] is very similar to the QCM

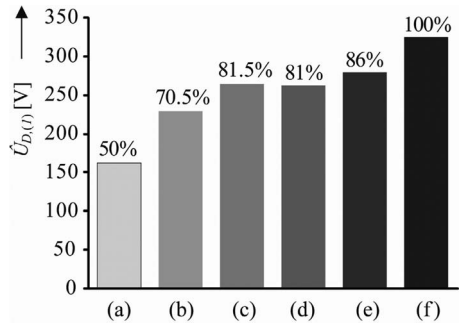

Fig. 7. Maximum applicable fundamental amplitude of drive voltage $u_{D(1)}$ achieved with the (a) CCM (b) SCM (c) QCM (d) THM (e) TQM, and (f) FBM method.

[cf., Fig. 6(b)], since it is mainly determined by the square common bridge leg.

D. Comparison of Modulation Schemes

In order to compare the effect of the presented modulation schemes, the fundamental harmonic of the voltage applied to the drive coil L_D is calculated for each of the average voltages $\overline{u}_{D1}(t)$ shown in Figs. 3, 4, and 7. The comparison is done with the value obtained with the state-of-the-art full-bridge modulation (FBM) method implemented for the control of the topology in Fig. 1(a). As shown in Fig. 7 is the maximum amplitude achievable with the CCM method half of that which results from FBM. Furthermore, the maximum voltage that can be obtained with the optimal modulation scheme (TQM) for the interleaved half-bridge topology is 86% of that resulting with FBM and the state-of-the-art full-bridge topology [cf., Fig. 1(b)].

IV. Analysis of Speed Oscillations Due to Harmonic Injection

In the previous sections, starting from the purely sinusoidal modulation concepts (CCM, SCM), gradually higher harmonics have been superposed in order to increase the modulation depth. However, as already stated before, this results in progressively more distorted current waveforms.

In this paragraph, it shall be investigated to which extent this higher harmonic distortion takes influence on speed oscillations in the pump system which then results in higher vibrations of the impeller which limits its lifetime. Latter is a known issue in not only the design of bearingless but also in the design of conventional pumps [19]. Since the power requirements are much lower for the bearing system it can be operated with CCM as described in Section III-A. Variations in the available voltage of the bearing system would have to be compensated by the controller, which can be challenging particularly for high rotation speeds and can lead to vibrations and/or instabilities. Thus, the employment of CCM ensures that no distortions appear for the magnetic suspension. Hence, influence of higher harmonics on the operation of the pump is only analyzed for the drive system in the following.

In a first step, a reference operating point of the pump and the motor is chosen under steady-state conditions where the impeller is held at constant angular speed of ω_0. Furthermore, the pump is working against a given load $P_{hydr} = P_0$. The average torque M_0 that is exerted by the average torque current $\bar{i}_{q0}$ on the impeller is in equilibrium with all dynamic and frictional forces

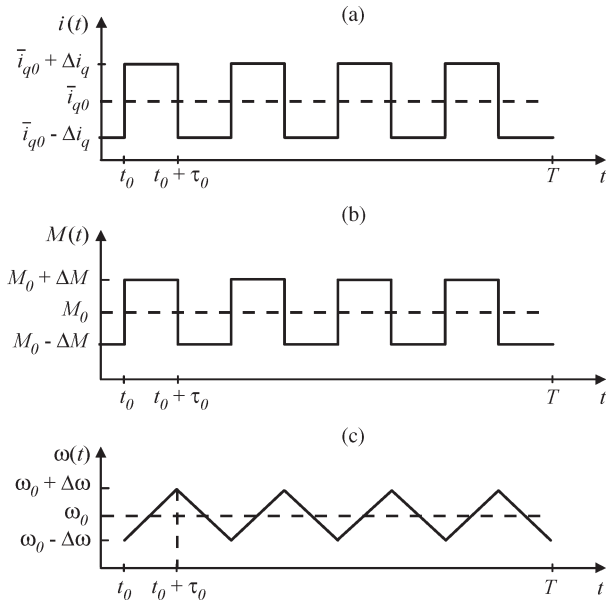

Fig. 8. Estimated worst case current waveform of the torque generating current $i_q(t)$, the resulting torque $M(t)$ and the subsequent speed $\omega(t)$ of the motor.

$$M_0 = c_m \cdot \bar{i}_{q0} \tag{14}$$

where c_m is the torque constant of the motor. With this constant torque M_0, the impeller rotates with a constant rotation speed ω_0.

A distorted worst case torque current $i_q(t)$ flowing through each of the four drive coils can be represented by a square wave function with an amplitude Δi_q around the average value of $\bar{i}_q(0)$ as it is shown in Fig. 8. For this case, the speed ramps up during the time while a higher torque $M_0 + \Delta M$ with

$$\Delta M = c_M \cdot \Delta i_q \tag{15}$$

is applied and analogously ramps down while $M_0 - \Delta M$ is applied (cf., Fig. 8), whereby a speed oscillation $\pm\Delta\omega$ around an average value of ω_0 occurs. The rise time τ_0 of this oscillation is given by twice the number of drive coils, which each causes a torque disturbance ΔM, per mechanical revolution. Since each of the two drive windings L_{D1} and L_{D2} [cf., Fig. 1(b)] is built up with two coils connected in series, the number of drive coils arranged over one full circle is $n_{drc} = 4$, and the characteristic time constant is then given by

$$\tau_0 = \frac{2\pi}{\omega_0} \cdot \frac{1}{2n_{drc}}. \tag{16}$$

A cutoff frequency ω_0 is then defined by applying a criterion according to which the time scale of this square-wave function

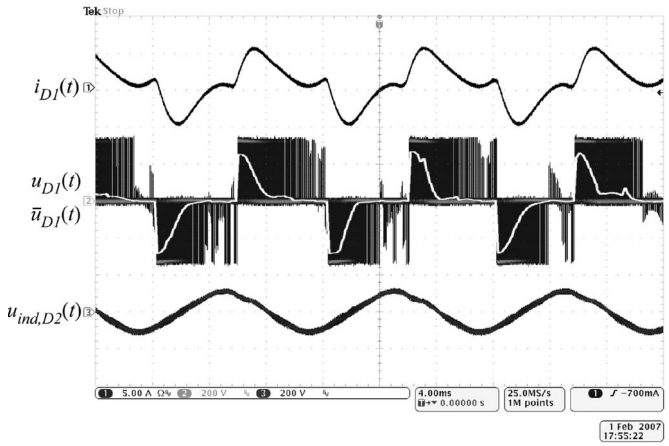

Fig. 9. Experimental results for the induced voltage for highly distorted drive currents obtained with TQM. Time behavior of drive current i_{D1}, switched voltage u_{D1} and average voltage $\overline{u}_{D1}$ across drive coil L_{D1} and induced voltage $u_{ind,D2}$ in drive L_{D2}. Current scale: i_{D1}: 5 A/div, voltage scale: u_{D1}, $u_{ind,D2}$: 200 V/div, time scale: 4 ms/div.

must be smaller than a typical acceleration time of the impeller resulting from the torque characteristic given with

$$\tau_{acc} = \frac{\omega_0 \cdot J}{c_m \cdot \bar{i}_{q0}} > \tau_0 \tag{17}$$

where J is the geometrical moment of inertia and c_m is the torque constant of the motor. Implementing (16) into (17) and resolving the latter for ω_0 leads to

$$\omega_0 > \widetilde{\omega}\, \omega_0 > \sqrt{\pi} \cdot \tilde{\omega} \tag{18}$$

where

$$\widetilde{\omega} = \sqrt{\frac{\pi \cdot c_m \cdot \bar{i}_{q0}}{n_{drc} \cdot J}}. \tag{19}$$

The motor investigated here has a torque constant $c_m = 0.205$ Vs. With a reference current of $\bar{i}_{q0} = 4$ A and an estimated geometrical moment of inertia of $J = 300$ kg.mm^2, the reference frequency in (19) can be determined as $\widetilde{\omega} = 46.33$ rad/s. This result translates to a cutoff pump speed of

$$\frac{60}{2\pi} \cdot \frac{s}{\min} \cdot \omega_0 = n_0 > 442 \text{ r/min}. \tag{20}$$

Above this speed, the effects of higher harmonic components of the drive current on the constancy of the angular speed of the impeller are presumably attenuated significantly.

Experiments with the pump driven in single-phase operation under load have shown that at a speed of $n = 5000$ r/min, where the pump is already operating with a reasonable hydraulic power, the induced voltage $u_{ind,D2}(t)$ measured across the open drive coil L_{D2} is sinusoidal as shown in Fig. 9 although the current is obviously distorted significantly. In addition to the induced voltage in the drive phase 2 ($u_{ind,D2}(t)$), the switched voltage $u_{D1}(t)$) and average voltage $\overline{u}_{D1}(t)$ across the drive phase 1 are shown in this figure as well.

In order to underline this result of a constant speed of the impeller, the output signal of the hall sensor used to measure the speed of the impeller is undertaken a Fourier analysis. This is done at a speed of 6000 r/min, a flow of 60 L/min, and an output pressure of 1.4 bar. The results are shown in Fig. 10 for an operation of the pump at the beforehand mentioned operating point with the SCM (a) and TQM (b) method. The Fourier analysis leads to very similar results for both modulation methods and thereby shows that the higher harmonics implemented in the TQM method do not lead to a speed oscillation. In both cases a small third harmonic (about 2% of the fundamental signal) can be seen, which is caused by the inhomogeneity of the permanent magnet, which generates a field which is not of perfect sinusoidal shape.

Summing up, it can be concluded that the impeller is rotating at constant speed despite of higher harmonics superposed to the drive current.

V. Maximum Achievable Drive Power

The maximum applicable drive power to each of the two motor phases is depending on the induced voltage $\hat{u}_{ind}$ and the current $\hat{i}_{D(1)}$, which is in phase with $\hat{u}_{ind}$ for the field oriented control (cf., Fig. 11), flowing through that drive coil.

Due to the fact that the induced voltage does not contain higher harmonics (see Section IV), only the fundamental harmonic of that current needs to be considered for the calculation of the drive power.

Doing this, leads to the following equation for the motor drive power P_D of one drive winding:

$$P_D = u_{ind,rms} \cdot i_{D,(1),rms} \tag{21}$$

where $i_{D,(1),rms}$ is the rms value of the fundamental harmonic of the current in the drive phase one and $u_{ind,rms}$ is the rms value of the induced voltage in that winding, which is experimentally measured to $u_{ind,rms} = 15.8\ \mathrm{V}/1000$ r/min for the here employed motor.

According to the phasor diagram shown in Fig. 11, the following equation is given:

$$\left(\hat{u}_{ind} + R_D \cdot \hat{i}_{D(1)}\right)^2 + \left(\omega_{el} \cdot L_D \cdot \hat{i}_{D(1)}\right)^2 = \hat{u}_{D(1)}^2 \tag{22}$$

where ω_{el} is the rotating speed of the impeller in radians per second.

Solving (22) for $\hat{i}_{D1}$ results in

$$\hat{i}_{D(1)} = \frac{-\hat{u}_{ind} \cdot R_D \pm \sqrt{(R_D^2 + \omega_{el}^2 \cdot L_D^2) \cdot \hat{u}_{D(1)}^2 - \omega_{el}^2 \cdot L_D^2 \cdot \hat{u}_{ind}^2}}{R_D^2 + \omega_{el}^2 \cdot L_D^2}. \tag{23}$$

With (21) and (23), the total drive power of the two drive phases can now be calculated for different rotating speeds. In Fig. 12, the maximal achievable drive power depending on the chosen modulation scheme is shown for $U_{dc} = 320$ V, $m_{\max} = 0.95$, and $I_{D,\max,rms} = 10$ A. There, the methods that have been presented in Section III are compared to the state-of-the-art FBM operated with the topology in Fig. 1(a). For these calculations, a motor with an inductance $L_D = 35$ mH and $R_D = 720$ mΩ per drive phase is employed.

As shown in Fig. 12, above a rotating speed of 6500 r/min, the CCM method can no longer be utilized since the induced

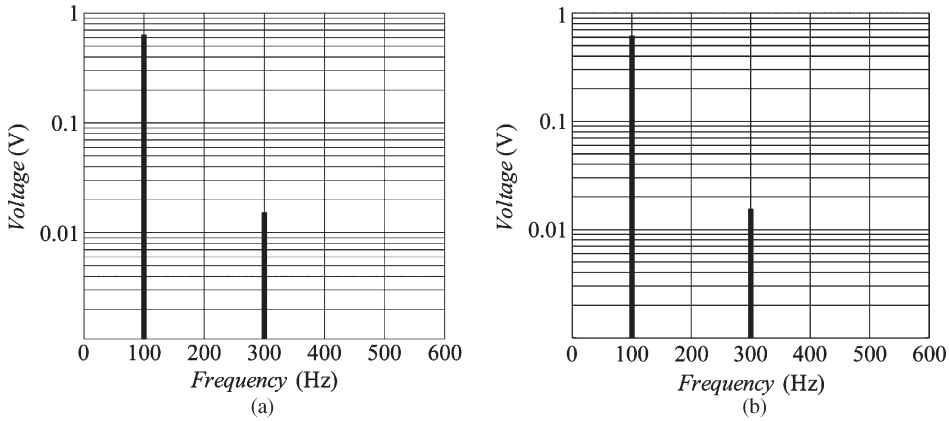

Fig. 10. Fourier analysis of the output signal of the hall sensor used to measure the speed of the impeller for SCM (a) and TQM (b) modulation.

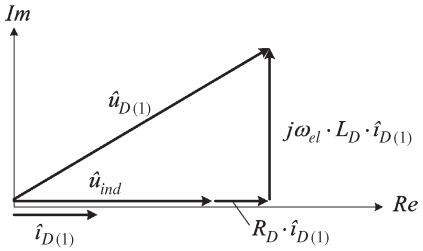

Fig. 11. Phasor diagram of the equivalent electrical circuit of one drive phase with the basic phasor orientation.

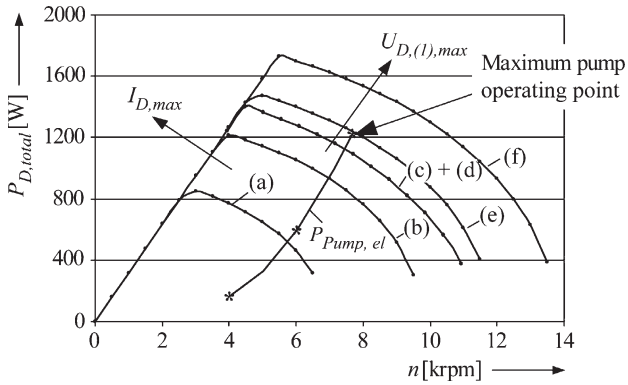

Fig. 12. Total achievable drive power for the motor with (a) CCM (b) SCM (c) QCM (d) THM (e) TQM, and (f) FBM method.

voltage is becoming higher than the maximum applicable voltage, whereas with SCM still three times the power can be delivered to the drive system at this speed. The power rating can be further improved when switching to an increased modulation depth by using the QCM, THM (which have the same performance), or finally the TQM method.

The maximum hydraulic power of the pump is limited to a flow of 100 L/min with a pressure of 3.6 bar [20]. This is achieved at a speed of $n = 8000$ r/min, and the necessary drive power required to operate the pump at this point is 1190 W. According to Fig. 12, this can be achieved by the TQM method with no performance decrease compared to the conventional full-bridge topology with its modulation. Furthermore, it can be seen that the achievable drive power is limited for lower rotational speeds by the maximum allowable drive current. On the other hand, for higher speeds the maximum applicable drive voltage that is ensured by the respective modulation scheme limits the achievable drive power.

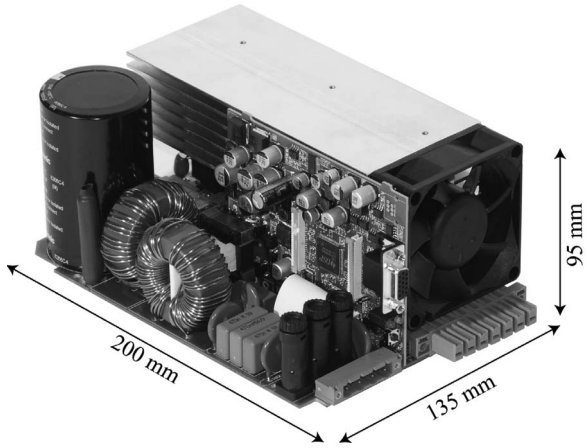

Fig. 13. Prototype of the 1.5-kW interleaved half-bridge converter with two integrated three-phase power modules for the control of the drive and bearing system.

VI. Experimental Verification

The proposed modulation schemes have been implemented on a DSP and tested with a prototype (cf., Fig. 13) of a 1.5-kW converter. This system is built up with two integrated half-bridge power modules [21] for the drive and bearing system and is operated from a single phase mains voltage. Each IGBT of these modules has a maximum peak current rating of 30 A. The switching frequency of the drive and bearing system is chosen to 18.3 kHz.

A. Verification of Modulation Schemes

In Fig. 14, the current and voltage waveforms in the drive system generated by the different modulation schemes are presented. The measured shapes of the drive currents i_{D1} and i_{D2} are in good agreement with the simulation results (cf., Figs. 3, 4, and 7).

Furthermore, tests with a bearingless pump system under load have been carried out in order to show the resulting maximum torque limits of the different modulation schemes.

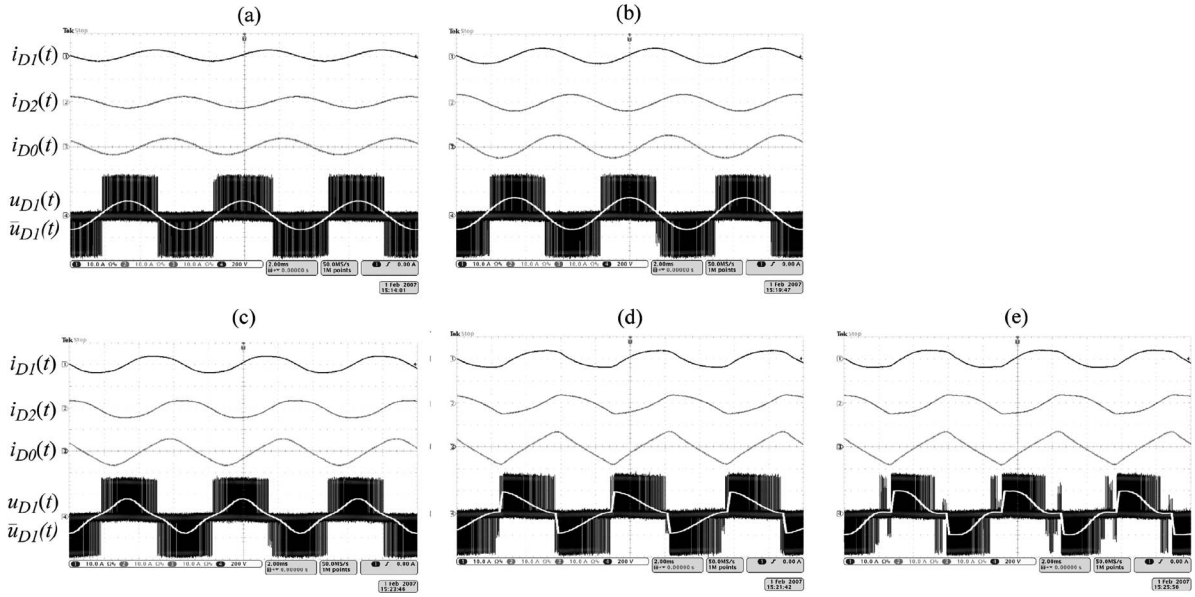

Fig. 14. Experimental results of the modulation schemes presented in Section III. (a) CCM. (b) SCM. (c) THM. (d) QCM. (e) TQM. Time behavior of drive currents i_{D1} and i_{D2}, common bridge leg current i_{D0}, switched voltage u_{D1}, and average voltage $\overline{u}_{D1}(t)$ of drive coil L_{D1}. Current scales: i_{D0}, i_{D1}, i_{D2}: 10 A/div. Voltage scale: u_{D1}: 200 V/div. Time scale: 2 ms/div.

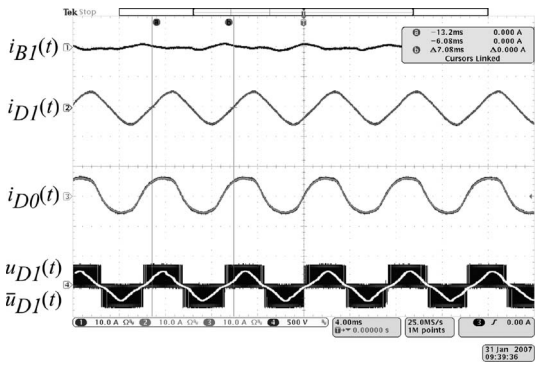

Fig. 15. Experimental results for the pump under operation employing the THM method with an impeller speed of 8500 r/min, a flow of 38.5 L/min, and resulting pressure of 4.5 bar. Time behavior of bearing current i_{B1}, drive current i_{D1}, common bridge leg current i_{D0}, switched voltage u_{D1}, and average voltage across $\overline{u}_{D1}(t)$ of drive L_{D1}. Current scales: i_{B1}, i_{D1}, i_{D0}: 10 A/div. Voltage scale: u_{D1}: 500 V/div. Time scale: 4 ms/div.

As an example, the result for the THM method is shown in Fig. 15. This allows it to rotate the impeller with a speed of 8500 r/min while regulating the flow to 38 L/min. The resulting output pressure is then 4.5 bar. The current i_{B1} in the bearing phase L_{B1}, the drive current i_{D1}, the common bridge leg current i_{D0}, as well as the switched voltage u_{D1} across the drive coil L_{D1} are shown in the aforesaid figure. As shown, the bearing current i_{B1} shown in that figure is relatively small compared to the drive current i_{D1}, and thus, the CCM method is sufficient to control that current.

Thus, the control of the bearing system with the CCM method still ensures a sufficient performance over the whole operating range of the pump, while for the control of the drive system for higher power and/or rotation speeds the presented more advanced modulation techniques have to be employed (cf., Fig. 12). For example, the shown operating point in Fig. 15 could not be achieved by the CCM or SCM method.

VII. Summary

In this paper, novel modulation concepts for the control of a two-phase BSM pump operated with the interleaved half-bridge topology have been presented. Starting with a CCM, more advanced modulation concepts with the superposition of higher harmonics were then presented. The proposed modulation schemes are compared based on the maximum achievable drive power for the motor. With the highest level of harmonic superposition, the maximum voltage applicable to the drive phases is 86% of that obtained with the state-of-the-art full-bridge topology and its control method. As shown in analytical calculations, these higher harmonics in the drive current do not have an impact on the constant speed of the impeller and thus on the constant output flow of the pump. This was finally verified by measurements on a pump system with a 1.5-kW converter realized with integrated half-bridge power modules.

References

[1] R. Schöb, "The future in hand—A new type of pump for delicate fluids," *World Pumps*, no. 430, Jul. 2002.
[2] J. Bichsel, "Beiträge zum lagerlosen Elektromotor," Ph.D. dissertation, Elect. Eng. Des. Lab., ETH Zurich, Zurich, Switzerland, 1990.
[3] M. Neff, N. Barletta, and R. Schöb, "Magnetically levitated centrifugal pump for highly pure and aggressive chemicals," in *Proc. PCIM Conf.*, Nuremberg, Germany, Jun. 6–8, 2000.
[4] M. T. Bartholet, T. Nussbaumer, P. Dirnberger, and J. W. Kolar, "Novel converter concept for bearingless slice motor systems," in *Conf. Rec. IEEE IAS Annu. Meeting*, 2006, vol. 5, pp. 2496–2502.
[5] B. Francois and A. Bouscayrol, "Design and modelling of a five-phase voltage-source inverter for two induction motors," in *Proc. Eur. Conf. Power Electron. Appl. (EPE)*, Lausanne, Switzerland, 1999, CD-ROM, Paper 626.
[6] C. B. Jacobina, O. I. da Silva, E. C. dos Santos, Jr., and A. M. N. Lima, "Reduced switch count multi-motor drive systems," in *Proc. IEEE IEMDC*, San Antonio, TX, 2005, pp. 1858–1862.
[7] C. B. Jacobina, M. B. de Rossiter Corrêa, A. M. N. Lima, and E. C. R. da Silva, "AC motor drive systems with a reduced switch count converter," *IEEE Trans. Ind. Appl.*, vol. 39, no. 5, pp. 1333–1342, Sep./Oct. 2003.

[8] M. B. de Rossiter Corrêa, C. B. Jacobina, A. M. N. Lima, and E. R. C. da Silva, "A three-leg voltage source inverter for two-phase AC motor drive systems," *IEEE Trans. Power Electron.*, vol. 17, no. 4, pp. 517–523, Jul. 2002.
[9] P. Delarue, A. Bouscayrol, and B. Francois, "Control implementation of a five-leg voltage-source-inverter supplying two three-phase induction machines," in *Proc. IEEE IEMDC*, Madison, WI, 2003, pp. 1909–1915.
[10] F. Blaabjerg, F. Lungeanu, K. Skaug, and M. Tonnes, "Two-phase induction motor drives," *IEEE Ind. Appl. Mag.*, vol. 10, no. 4, pp. 24–32, Jul./Aug. 2004.
[11] D. G. Holmes and A. Kotsopoulos, "Variable speed control of single and two phase induction motors using a three phase voltage source inverter," in *Conf. Rec. IEEE IAS Annu. Meeting*, 1993, vol. 1, pp. 613–620.
[12] C.-M. Young, C.-C. Liu, and C.-H. Liu, "New inverter driven design and control method for two-phase induction motor drives," *Proc. Inst. Elect. Eng.—Electr. Power Appl.*, vol. 143, no. 6, pp. 458–466, Nov. 1996.
[13] M. J. Meco-Gutiérrez, F. Pérez-Hidalgo, F. Vargas-Merino, and J. R. Heredia-Larrubia, "Pulse width modulation technique with harmonic injection and frequency modulated carrier: Formulation and application to an induction motor," *IET Electr. Power Appl.*, vol. 1, no. 5, pp. 714–726, Sep. 2007.
[14] S. R. Bowes, D. Holliday, and S. Grewal, "Comparison of single-phase three-level pulse width modulation strategies," *Proc. Inst. Elect. Eng.—Electr. Power Appl.*, vol. 151, no. 2, pp. 205–214, Mar. 2004.
[15] S. R. Bowes and D. Holliday, "Comparison of pulse-width-modulation control strategies for three-phase inverter systems," *Proc. Inst. Elect. Eng.—Electr. Power Appl.*, vol. 153, no. 4, pp. 575–584, Jul. 2006.
[16] N. Mohan, T. M. Undeland, and W. P. Robbins, *Power Electronics: Converters, Applications and Design*, 3rd ed. New York: Wiley, 2003, pp. 215–218.
[17] E. R. Benedict and T. A. Lipo, "Improved PWM modulation for a permanent-split capacitor motor," in *Conf. Rec. IEEE IAS Annu. Meeting*, 2000, vol. 3, pp. 2004–2010.
[18] J. A. Houldsworth and D. A. Grant, "The use of harmonic distortion to increase the output voltage of a three-phase PWM inverter," *IEEE Trans. Ind. Appl.*, vol. IA-20, no. 5, pp. 1224–1228, Sep./Oct. 1984.
[19] *Sulzer Centrifugal Pump Handbook*, 2nd ed., Sulzer Pumps, Elsevier Adv. Technol., Oxford, U.K., 1998.
[20] Levitronix Pumps. [Online]. Available: http://www.levitronix.com
[21] Datasheet, International Rectifier: Integrated Hybrid IC IRAMY30UP60B.

Martin T. Bartholet (M'09) received the M.Sc. and Ph.D. degrees in electrical engineering from the Swiss Federal Institute of Technology (ETH) Zurich, Zurich, Switzerland, in 2004 and 2008, respectively. During his studies, he dealt with power electronics, machines, and magnetic bearings. For his Master's Thesis, he was at Chalmers University of Technology, Göteborg, Sweden, where he worked on wind turbines. During his Ph.D. studies, he performed research on magnetically levitated motors and pumps for the semiconductor industry.

Since August 2008, he has been with Celeroton AG, Zurich, where he is a Co-founder and is currently working on ultra-high-speed electric drive systems.

Thomas Nussbaumer (S'02–M'06) was born in Vienna, Austria, in 1975. He received the M.Sc. degree (with honors) in electrical engineering from the University of Technology Vienna, Vienna, Austria, in 2001, and the Ph.D. degree from the Power Electronic Systems (PES) Laboratory, Swiss Federal Institute of Technology (ETH) Zurich, Zurich, Switzerland, in 2004.

From 2001 to 2006, he was with the PES, where he conducted research on modeling, design, and control of three-phase rectifiers, power factor correction techniques, and electromagnetic compatibility. Since 2006, he has been with Levitronix GmbH, Zurich, Switzerland, where he is currently working on bearingless motors, magnetic levitation, and permanent-magnet motor drives for the semiconductor and biotechnology industry. His current research is focused on compact and high-performance mechatronic systems including novel power electronics topologies, control techniques, drive systems, sensor technologies, electromagnetic interference (EMI), and thermal aspects.

Daniel Krähenbühl (S'08) received the M.Sc. degree in electrical engineering from the Swiss Federal Institute of Technology Zurich, Zurich, Switzerland, in 2007, where he is working toward the Ph.D. degree in the Power Electronic Systems Laboratory, focusing on high-speed electrical drives and generator systems.

During his studies, he dealt with electrical drive systems, power electronics, and very large scale integration.

Franz Zürcher (S'08) received the M.Sc. degree in electrical engineering from the Swiss Federal Institute of Technology Zurich, Zurich, Switzerland, in 2007, where he is working toward the Ph.D. degree in the Power Electronic Systems Laboratory since 2008, focusing on high-acceleration magnetically levitated motors.

His focus during his studies has been on mechatronics, power electronics, and microelectronics. In spring 2007, he concluded his master's thesis in which he designed and realized a 1.5-kW converter for bearingless motors in cooperation with the company Levitronix GmbH.

Johann W. Kolar (M'89–SM'04–F'10) received the Ph.D. degree (*summa cum laude/promotio sub auspiciis praesidentis rei publicae*) from the University of Technology Vienna, Vienna, Austria.

Since 1984, he has been working as an independent international consultant in close collaboration with the University of Technology Vienna, in the fields of power electronics, industrial electronics, and high-performance drives. He has proposed numerous novel PWM converter topologies, and modulation and control concepts, e.g., the VIENNA Rectifier and the Three-Phase AC-AC Sparse Matrix Converter. He has published over 350 scientific papers in international journals and conference proceedings and has filed 75 patents. He was appointed Professor and Head of the Power Electronic Systems Laboratory at the Swiss Federal Institute of Technology (ETH) Zurich, Zurich, Switzerland, on February 1, 2001. The focus of his current research is on ac–ac and ac–dc converter topologies with low effects on the mains, e.g., for power supply of data centers, More-Electric-Aircraft and distributed renewable energy systems. Further main areas of research are the realization of ultra-compact and ultra-efficient converter modules employing latest power semiconductor technology (SiC), novel concepts for cooling and EMI filtering, multi-domain/multi-scale modeling/simulation and multi-objective optimization, physical-model-based lifetime prediction, pulsed power, bearingless motors, and Power MEMS.

Dr. Kolar received the Best TRANSACTIONS Paper Award of the IEEE Industrial Electronics Society in 2005, the Best Paper Award of the ICPE'07 and the 1st Prize Paper Award of the IEEE IAS IPCC in 2008. He also received an Erskine Fellowship from the University of Canterbury, New Zealand, in 2003. In 2006, the European Power Supplies Manufacturers Association (EPSMA) recognized the Power Electronics Systems Laboratory of ETH Zurich as the leading academic research institution in Europe. He a member of the IEEJ and of Technical Program Committees of numerous international conferences in the field (e.g., Director of the Power Quality Branch of the International Conference on Power Conversion and Intelligent Motion). From 1997 through 2000, he served as an Associate Editor of the IEEE TRANSACTIONS ON INDUSTRIAL ELECTRONICS and, since 2001, he has an been an Associate Editor of the IEEE TRANSACTIONS ON POWER ELECTRONICS. Since 2002, he has also been an Associate Editor of the *Journal of Power Electronics of the Korean Institute of Power Electronics* and a member of the Editorial Advisory Board of the *IEEJ Transactions on Electrical and Electronic Engineering*.